NASA Technical Memorandum 4040
Part 1



# Pressure Distributions From Subsonic Tests of an Advanced Laminar-Flow-Control Wing With Leading- and Trailing-Edge Flaps

Zachary T. Applin and Garl L. Gentry, Jr.



JULY 1988

NASA

NASA Technical Memorandum 4040
Part 1

# Pressure Distributions From Subsonic Tests of an Advanced Laminar-Flow-Control Wing With Leading- and Trailing-Edge Flaps

Zachary T. Applin and Garl L. Gentry, Jr.
*Langley Research Center*
*Hampton, Virginia*

National Aeronautics
and Space Administration

**Scientific and Technical
Information Division**

**1988**

## Contents

### Part 1



### Part 2*



* Part 2 is published under separate cover and consists of pages 29 to 363.

## Summary

An unswept, semispan wing model equipped with full-span leading- and trailing-edge flaps was tested in the Langley 14- by 22-Foot Subsonic Tunnel to determine the effect of high-lift components on the aerodynamics of an advanced laminar-flow-control (LFC) airfoil section. Chordwise pressure distributions near the midsemispan were measured for four configurations: cruise, trailing-edge flap only, and trailing-edge flap with a leading-edge Krueger flap of either 0.10 or 0.12 chord. Part 1 of this report presents a representative sample of the plotted pressure distribution data for each configuration tested. Part 2 (under separate cover) presents the entire set of plotted and tabulated pressure distribution data. The data are presented without analysis.

## Introduction

In recent years, NASA has been actively involved in the Aircraft Energy Efficiency (ACEE) program to improve the energy efficiency of modern jet transport aircraft. The laminar-flow-control (LFC) project is one element of this program that is concerned primarily with the application of advanced concepts to improve wing performance through the use of active boundary-layer control to provide increased laminar flow. Laminar flow over major portions of aircraft wings has long been known to reduce the skin-friction drag and thereby improve aerodynamic performance and fuel economy. So far, however, natural laminar flow has proven to be difficult to obtain in commercial operation with transport aircraft because of constraints such as surface roughness, sweep effects, and noise. As a result, active flow-control concepts are being studied to sustain the laminar boundary layer. The new airfoils being designed to facilitate laminar flow in cruise need to be examined to assess their high-lift capabilities using current flap concepts. The purpose of this investigation was to determine the performance of such a laminar-flow airfoil when fitted with leading- and trailing-edge flaps.

A semispan rectangular-wing model was fabricated and tested in the Langley 14- by 22-Foot Subsonic Tunnel to determine the aerodynamic performance of a high-lift system on an unswept LFC wing. The model had a 39.37-in. chord and 118.11-in. semispan, and it incorporated a slightly modified version of the NASA advanced LFC airfoil section presented in references 1 to 3.

The high-lift system used on the model consisted of both leading- and trailing-edge flaps. The model had two different (0.10-chord and 0.12-chord) full-span leading-edge flap configurations and one full-span trailing-edge flap with a chord equal to 0.25 chord. The model also had a single chordwise row of surface pressure taps located near the midsemispan location. Measurements of the surface pressure distribution were obtained at free-stream Mach numbers of 0.10 and 0.14 over a range of angles of attack. This two-part report presents the tabulated and plotted pressure distribution data obtained during the investigation. Part 1 of this report presents a representative sample of the plotted pressure distribution data for each configuration tested (tables 1 to 6 and figs. 1 to 7). Part 2 (under separate cover) presents the entire set of plotted and computer-tabulated pressure distribution data (tables 7 to 447 and figs. 8 to 31). The data are presented without analysis.

## Symbols

All measurements and calculations were made in U.S. Customary Units. The parenthetic expression listed next to a symbol is the computer printout equivalent of that symbol and is used in the data listings in the tables in part 2.

| | | |
|---|---|---|
| $b$ | | wing semispan, 118.11 in. |
| $C_p$ | (CP) | static pressure coefficient, $(p_s - p_\infty)/q_\infty$ |
| $c$ | (C) | reference wing chord, 39.37 in. |
| $M$ | | free-stream Mach number |
| $p_s$ | | surface static pressure, $lb/ft^2$ |
| $p_\infty$ | | free-stream static pressure, $lb/ft^2$ |
| $q_\infty$ | | free-stream dynamic pressure, $lb/ft^2$ |
| $R$ | | Reynolds number, based on wing chord |
| $x, y, z$ | (X) | coordinates of wing pressure taps in wing reference axis system, in. |
| $\alpha$ | | angle of attack of model reference line, positive nose up, deg |
| $\delta_{LE}$ | | leading-edge flap-deflection angle, positive for flap trailing edge down, deg |
| $\delta_{TE}$ | | trailing-edge flap-deflection angle, positive for flap trailing edge down, deg |

Abbreviations:

| | |
|---|---|
| L.E. | leading edge |
| T.E. | trailing edge |
| WRP | wing reference plane |

## Test Setup

This investigation was conducted in the Langley 14- by 22-Foot Subsonic Tunnel, which is a closed, single-return, atmospheric wind tunnel with a test section 14.50 ft high by 21.75 ft wide by 50.00 ft long. (See ref. 4.) The test-section speed is continuously variable from 0 to 200 knots.

The tunnel is equipped with a floor boundary-layer removal system located 8.2 ft upstream of the wing leading edge and extending laterally across the floor of the test section between the tunnel walls. The boundary-layer thickness of the empty test section is reduced from 1.5 ft to approximately 1.6 in. at the wing location when the system is in operation. The wing was mounted vertically on a 15.8-ft-diameter turntable, which could be rotated throughout the angle-of-attack range of the wing.

The rectangular wing had a semispan of 118.11 in. and a 39.37-in. chord; it incorporated a slightly modified version of the NASA advanced LFC airfoil section presented in references 1 to 3. The modifications included shifting the lower-surface lobe rearward 0.02 chord and slightly altering the trailing-edge camber. These modifications allowed sufficient length in the chordwise direction, forward of the lower-surface lobe, for storage of a Krueger-type flap of up to 0.12 chord. A Krueger-type flap was chosen because possible surface discontinuities (i.e., steps, gaps, etc.) are on the lower-surface leading-edge region where favorable pressure gradients are generated. (See ref. 1.) No analysis has been made of the internal volume required for storage of an appropriate deployment mechanism. The primary purpose of this investigation was to determine the effect of the high-lift system on subsonic wing aerodynamics. Development and maintenance of significant amounts of laminar flow for this mode of operation may prove to be impractical. Consequently, no provisions were made to incorporate an LFC suction system into the present model.

The basic airfoil could be modified by installing either a $0.10c$ or $0.12c$ full-span leading-edge Krueger flap and by adding a full-span $0.25c$ trailing-edge flap. A sketch of the wing planform is presented in figure 1. All components of this semispan model had rounded tips. A single row of orifices (taps) located at $2y/b = 0.44$ was used to obtain surface pressure distributions. Coordinates of the wing airfoil section in both the cruise and high-lift configurations are given in terms of surface pressure tap locations in tables 1 and 2, respectively. The coordinates of the pressure taps are presented in table 3 for the trailing-edge flap and in table 4 for the two leading-edge flaps. Section contours of the configurations tested during this investigation are shown in figure 2. The high-lift components were positioned using the definitions for deflection, gap, and overlap presented in reference 5. For the trailing-edge flap, the gap and overlap were $0.02c$ and $0.00c$, respectively. For both leading-edge flaps, the gap and overlap were $0.12c$ and $0.16c$, respectively. These settings were used for all deflection angles tested in this investigation. Photographs of the wing model installed in the tunnel are presented in figure 3.

The wing was fabricated from solid aluminum by a numerically controlled milling machine. The resultant surface contour was within $\pm 0.005$ in. of the specified airfoil coordinates. Surface pressure tubes were routed internally to pressure instrumentation located below the tunnel floor. For configurations with the trailing-edge flap installed, the cruise trailing edge was replaced by a cove section, which had support brackets and pressure-tube routing recesses for the flap pressure tubes. Leading-edge flaps were supported by brackets mounted on the lower surface of the leading edge of the wing. Pressure tubes from the high-lift components were routed externally along the support brackets to the main component. These tubes were then routed internally through the main component to pressure instrumentation located below the tunnel floor. The external tubes were tightly taped to the flap brackets and streamlined with the use of modeling clay to produce a smooth aerodynamic surface. Modeling clay was also used to streamline the remaining flap brackets not used to route pressure tubes. Spanwise locations of the flap-bracket centerlines are given in table 5.

A thin boundary-layer transition strip was applied using No. 60 carborundum grit for all configurations. The transition roughness was sized according to reference 6. These transition strips were located on both the upper and lower surfaces at the 0.05 local chord station on each component and extended across the entire span.

Pressure measurements were obtained with an electronically scanned pressure (ESP) system. This system consisted of modules that contained a 720-psf-range silicon pressure transducer for every pressure orifice. Additional electronics were used to operate these transducers as 144-psf-range transducers. The manufacturer's quoted accuracy for this system was $\pm 0.5$ psf. These transducers were calibrated

on-line, a procedure that was used often in order to maintain a high degree of accuracy by accounting for the variation of tunnel temperature on the transducer. When a data point was measured, each of the pressure transducers was scanned electronically, thus acquiring all pressure data at essentially the same time.

## Test Procedure

The model was tested in four different configurations: (1) cruise, (2) trailing-edge flap only ($\delta_{TE} = 15°$), (3) trailing-edge flap with $0.10c$ leading-edge flap ($\delta_{TE} = 15°$ and $30°$; $\delta_{LE} = -50°, -55°$, and $-60°$), and (4) trailing-edge flap with $0.12c$ leading-edge flap ($\delta_{TE} = 15°$ and $30°$; $\delta_{LE} = -50°$ and $-55°$). All the high-lift components were full span. The angle-of-attack range varied with model configuration and was limited by the load capacity and stability of the mounting system. The specific angle-of-attack range for each configuration is presented in table 6. Test-section dynamic pressures of 15 and 30 psf ($M = 0.10$ and 0.14, respectively) were used throughout the investigation, which provided reference chord Reynolds numbers of $2.36 \times 10^6$ and $3.33 \times 10^6$, respectively.

Model angle-of-attack variation was accomplished by yawing the tunnel-floor turntable. Since the model was mounted perpendicular to the tunnel floor, yaw changes for the turntable provided angle-of-attack variation for the model. The yaw angle of the turntable was detected by a digital shaft encoder geared to the turntable drive mechanism. This system provided an angle-of-attack accuracy to within $\pm 0.02°$. A correction for blockage effects on the model was applied to the free-stream dynamic pressure by using the method described in reference 7. A correction for jet-boundary effects was applied to the angle of attack by using the method described in reference 8.

## Presentation of Results

This two-part report presents the tabulated and plotted pressure distribution data depicting the effect of full-span leading- and trailing-edge high-lift flaps on the wing pressures. The trailing-edge flap was installed for all the leading-edge flap configurations. A sample of the pressure distribution data for each of the four configurations is presented in figures 4 to 7 at $q_\infty = 30$ psf. The complete set of pressure distribution data is presented in part 2. Table 6 provides a synopsis of the various conditions for all the test data. Specifically, model configuration, test conditions, and corresponding run and figure numbers are presented in this table. Also presented in table 6 are the table numbers for part 2 of this report, which contains the computer-tabulated pressure distribution data.

NASA Langley Research Center
Hampton, Virginia 23665-5225
April 12, 1988

## References

1. Pfenninger, W.; Reed, Helen L.; and Dagenhart, J. R.: Design Considerations of Advanced Supercritical Low Drag Suction Airfoils. *Viscous Flow Drag Reduction*, Gary R. Hough, ed., American Inst. of Aeronautics & Astronautics, c.1980, pp. 249–271.
2. Harvey, W. D.; and Pride, J. D.: The NASA Langley Laminar Flow Control Airfoil Experiment. AIAA-82-0567, Mar. 1982.
3. Allison, Dennis O.; and Dagenhart, J. Ray: *Two Experimental Supercritical Laminar-Flow-Control Swept-Wing Airfoils.* NASA TM-89073, 1987.
4. Applin, Zachary T.: *Flow Improvements in the Circuit of the Langley 4- by 7-Meter Tunnel.* NASA TM-85662, 1983.
5. Morgan, Harry L., Jr.; and Paulson, John W., Jr.: *Low-Speed Aerodynamic Performance of a High-Aspect-Ratio Supercritical-Wing Transport Model Equipped With Full-Span Slat and Part-Span Double-Slotted Flaps.* NASA TP-1580, 1979.
6. Braslow, Albert L.; and Knox, Eugene C.: *Simplified Method for Determination of Critical Height of Distributed Roughness Particles for Boundary-Layer Transition at Mach Numbers From 0 to 5.* NACA TN 4363, 1958.
7. Herriot, John G.: *Blockage Corrections for Three-Dimensional-Flow Closed-Throat Wind Tunnels, With Consideration of the Effect of Compressibility.* NACA Rep. 995, 1950. (Supersedes NACA RM A7B28.)
8. Polhamus, Edward C.: *Jet-Boundary-Induced-Upwash Velocities for Swept Reflection-Plane Models Mounted Vertically in 7- by 10-Foot, Closed, Rectangular Wind Tunnels.* NACA TN 1752, 1948.

Table 1. Surface Pressure Tap Locations for Cruise Configuration

| Upper surface | |
|---|---|
| $x$, in. | $z$, in. |
| 0.0724 | 0.2047 |
| .2079 | .3622 |
| .4298 | .5079 |
| .7920 | .6654 |
| 1.1890 | .7913 |
| 1.7875 | .9409 |
| 2.3639 | 1.0630 |
| 3.1544 | 1.2008 |
| 3.9450 | 1.3189 |
| 4.7277 | 1.4213 |
| 5.5042 | 1.5079 |
| 6.4978 | 1.6102 |
| 7.4852 | 1.7008 |
| 8.4663 | 1.7756 |
| 9.8411 | 1.8661 |
| 11.8143 | 1.9724 |
| 13.7797 | 2.0512 |
| 17.7183 | 2.1339 |
| 21.6521 | 2.1181 |
| 25.5970 | 2.0000 |
| 27.5640 | 1.8937 |
| 29.5324 | 1.7402 |
| 31.5072 | 1.5276 |
| 33.2883 | 1.2559 |
| 35.0473 | .9291 |
| 36.6332 | .6181 |
| 37.7970 | .3701 |
| 38.5954 | .2008 |

| Lower surface | |
|---|---|
| $x$, in. | $z$, in. |
| 0 | 0 |
| .3835 | −.2283 |
| .7838 | −.2953 |
| 1.1732 | −.3543 |
| 1.7644 | −.4449 |
| 2.5509 | −.5669 |
| 3.3394 | −.6850 |
| 4.3161 | −.8346 |
| 5.3051 | −.9803 |
| 6.4898 | −1.2953 |
| 7.6650 | −1.8228 |
| 8.8491 | −2.2756 |
| 10.0387 | −2.5236 |
| 11.8055 | −2.7559 |
| 13.7753 | −2.9055 |
| 17.7192 | −2.9724 |
| 21.6548 | −2.7677 |
| 25.6013 | −2.2283 |
| 27.5584 | −1.7244 |
| 29.5269 | −1.1299 |
| 31.4947 | −.5354 |
| 33.0682 | −.0551 |
| 34.6318 | .1693 |
| 36.2100 | .2244 |
| 37.3927 | .1969 |
| 38.5836 | .0945 |
| 39.3624 | .0236 |

Table 2. Surface Pressure Tap Locations for High-Lift Configuration

| Upper surface | |
|---|---|
| $x$, in. | $z$, in. |
| 0.0724 | 0.2047 |
| .2079 | .3622 |
| .4298 | .5079 |
| .7920 | .6654 |
| 1.1890 | .7913 |
| 1.7875 | .9409 |
| 2.3639 | 1.0630 |
| 3.1544 | 1.2008 |
| 3.9450 | 1.3189 |
| 4.7277 | 1.4213 |
| 5.5042 | 1.5079 |
| 6.4978 | 1.6102 |
| 7.4852 | 1.7008 |
| 8.4663 | 1.7756 |
| 9.8411 | 1.8661 |
| 11.8143 | 1.9724 |
| 13.7797 | 2.0512 |
| 17.7183 | 2.1339 |
| 21.6521 | 2.1181 |
| 25.5970 | 2.0000 |
| 27.5640 | 1.8937 |
| 29.5324 | 1.7402 |
| 31.4924 | 1.5472 |
| 32.4702 | 1.4094 |
| 33.2612 | 1.2795 |
| 34.0315 | 1.1417 |

| Lower surface | |
|---|---|
| $x$, in. | $z$, in. |
| 0 | 0 |
| .3835 | −.2283 |
| .7838 | −.2953 |
| 1.1732 | −.3543 |
| 1.7644 | −.4449 |
| 2.5509 | −.5669 |
| 3.3394 | −.6850 |
| 4.3161 | −.8346 |
| 5.3051 | −.9803 |
| 6.4898 | −1.2953 |
| 7.6650 | −1.8228 |
| 8.8491 | −2.2756 |
| 10.0387 | −2.5236 |
| 11.8055 | −2.7559 |
| 13.7753 | −2.9055 |
| 17.7192 | −2.9724 |
| 21.6548 | −2.7677 |
| 25.6013 | −2.2283 |
| 27.5584 | −1.7244 |
| 29.4906 | −1.1220 |
| 30.6853 | −.6575 |
| 31.6770 | −.0315 |
| 32.4759 | .5079 |
| 33.0524 | .8425 |
| 33.6629 | 1.0433 |
| 34.2513 | 1.1024 |

Table 3. Surface Pressure Tap Locations for Trailing-Edge Flap

| Upper surface | |
|---|---|
| $x$, in. | $z$, in. |
| 0.1978 | 0.4961 |
| .5840 | .8386 |
| 1.1710 | 1.1024 |
| 2.3478 | 1.2677 |
| 3.5381 | 1.2480 |
| 5.1094 | 1.0079 |
| 6.6937 | .7008 |
| 8.2727 | .3661 |

| Lower surface | |
|---|---|
| $x$, in. | $z$, in. |
| 0 | 0 |
| .2033 | −.4291 |
| .5807 | −.6732 |
| 1.1691 | −.7559 |
| 1.7593 | −.5984 |
| 2.3631 | −.4173 |
| 3.5337 | −.0591 |
| 5.1106 | .1693 |
| 6.6900 | .2240 |
| 7.8735 | .1969 |
| 9.0439 | .0984 |
| 9.8379 | 0 |

Table 4. Surface Pressure Tap Locations for Leading-Edge Flaps

(a) 0.10$c$ leading-edge flap

| Upper surface | |
|---|---|
| $x$, in. | $z$, in. |
| 0.1035 | 0.2874 |
| .2969 | .5118 |
| .5365 | .6654 |
| .7872 | .7756 |
| 1.1845 | .8583 |
| 1.7797 | .8346 |
| 2.3661 | .6968 |
| 2.9495 | .4882 |
| 3.5506 | .2126 |

| Lower surface | |
|---|---|
| $x$, in. | $z$, in. |
| 0 | 0 |
| .1040 | −.2441 |
| .2973 | −.4094 |
| .5743 | −.4921 |
| .8860 | −.4922 |
| 1.1696 | −.4055 |
| 1.5777 | −.2205 |
| 1.9658 | −.0157 |
| 2.4654 | .1457 |
| 2.9431 | .1890 |
| 3.4362 | .1378 |
| 3.9335 | 0 |

(b) 0.12$c$ leading-edge flap

| Upper surface | |
|---|---|
| $x$, in. | $z$, in. |
| 0.1060 | 0.2677 |
| .3077 | .4764 |
| .5512 | .6181 |
| .7785 | .7323 |
| 1.1877 | .8346 |
| 1.7703 | .8661 |
| 2.3624 | .8031 |
| 2.9436 | .6654 |
| 3.5344 | .4882 |
| 4.1245 | .2667 |

| Lower surface | |
|---|---|
| $x$, in. | $z$, in. |
| 0 | 0 |
| .0894 | −.2165 |
| .2911 | −.3701 |
| .5856 | −.4724 |
| .8737 | −.5079 |
| 1.1635 | −.4764 |
| 1.5679 | −.3543 |
| 1.9634 | −.1890 |
| 2.4598 | .0157 |
| 2.9533 | .1457 |
| 3.4378 | .1850 |
| 3.9350 | .1654 |
| 4.4206 | .0787 |
| 4.7246 | 0 |

Table 5. Spanwise Locations of Flap-Bracket Centerlines

| Flap bracket | $y$, in. | $2y/b$ |
|---|---|---|
| 1 | 5.125 | 0.043 |
| 2 | 34.245 | .290 |
| 3 | 44.495 | .377 |
| 4 | 73.615 | .623 |
| 5 | 83.865 | .710 |
| 6 | 112.985 | .957 |

Table 6. Correlation of Configurations, Runs, Tables, and Figures for Parts 1 and 2

| Run | $R$ | $\delta_{LE}$, deg | $\delta_{TE}$, deg | Part 2 $C_p$ tables | $C_p$ figures | | Approximate range of $\alpha$, deg |
|---|---|---|---|---|---|---|---|
| | | | | | Part 1 | Part 2 | |
| Cruise configuration | | | | | | | |
| 19 | $2.36 \times 10^6$ | | | 19 to 32 | | 8 | −12 to 11 |
| 18 | 3.33 | | | 7 to 18 | 4 | 9 | −12 to 9 |
| Trailing-edge flap configuration | | | | | | | |
| 22 | $2.36 \times 10^6$ | | 15 | 47 to 62 | | 10 | −13 to 12 |
| 21 | 3.33 | | 15 | 33 to 46 | 5 | 11 | −13 to 8 |
| Trailing-edge flap with 0.10$c$ leading-edge flap configuration | | | | | | | |
| 48 | $2.36 \times 10^6$ | −50 | 15 | 254 to 272 | | 12 | −14 to 22 |
| 50 | 3.33 | ↓ | 15 | 273 to 290 | | 13 | −14 to 20 |
| 33 | 2.36 | ↓ | 30 | 63 to 81 | | 14 | −14 to 22 |
| 34 | 3.33 | ↓ | 30 | 82 to 94 | | 15 | −14 to 8 |
| 45 | 2.36 | −55 | 15 | 217 to 238 | | 16 | −14 to 28 |
| 46 | 3.33 | ↓ | 15 | 239 to 253 | | 17 | −14 to 14 |
| 36 | 2.36 | ↓ | 30 | 95 to 118 | | 18 | −14 to 27 |
| 37 | 3.33 | ↓ | 30 | 119 to 136 | 6 | 19 | −14 to 14 |
| 42 | 2.36 | −60 | 15 | 174 to 200 | | 20 | −14 to 29 |
| 43 | 3.33 | ↓ | 15 | 201 to 216 | | 21 | −14 to 14 |
| 39 | 2.36 | ↓ | 30 | 137 to 157 | | 22 | −14 to 26 |
| 40 | 3.33 | ↓ | 30 | 158 to 173 | | 23 | −14 to 16 |
| Trailing-edge flap with 0.12$c$ leading-edge flap configuration | | | | | | | |
| 52 | $2.36 \times 10^6$ | −50 | 15 | 291 to 312 | | 24 | −14 to 25 |
| 53 | 3.33 | ↓ | 15 | 313 to 329 | | 25 | −14 to 17 |
| 62 | 2.36 | ↓ | 30 | 411 to 432 | | 26 | −14 to 25 |
| 63 | 3.33 | ↓ | 30 | 433 to 447 | | 27 | −14 to 13 |
| 55 | 2.36 | −55 | 15 | 330 to 353 | | 28 | −14 to 25 |
| 56 | 3.33 | ↓ | 15 | 354 to 369 | | 29 | −14 to 16 |
| 58 | 2.36 | ↓ | 30 | 370 to 392 | | 30 | −14 to 25 |
| 60 | 3.33 | ↓ | 30 | 393 to 410 | 7 | 31 | −14 to 16 |

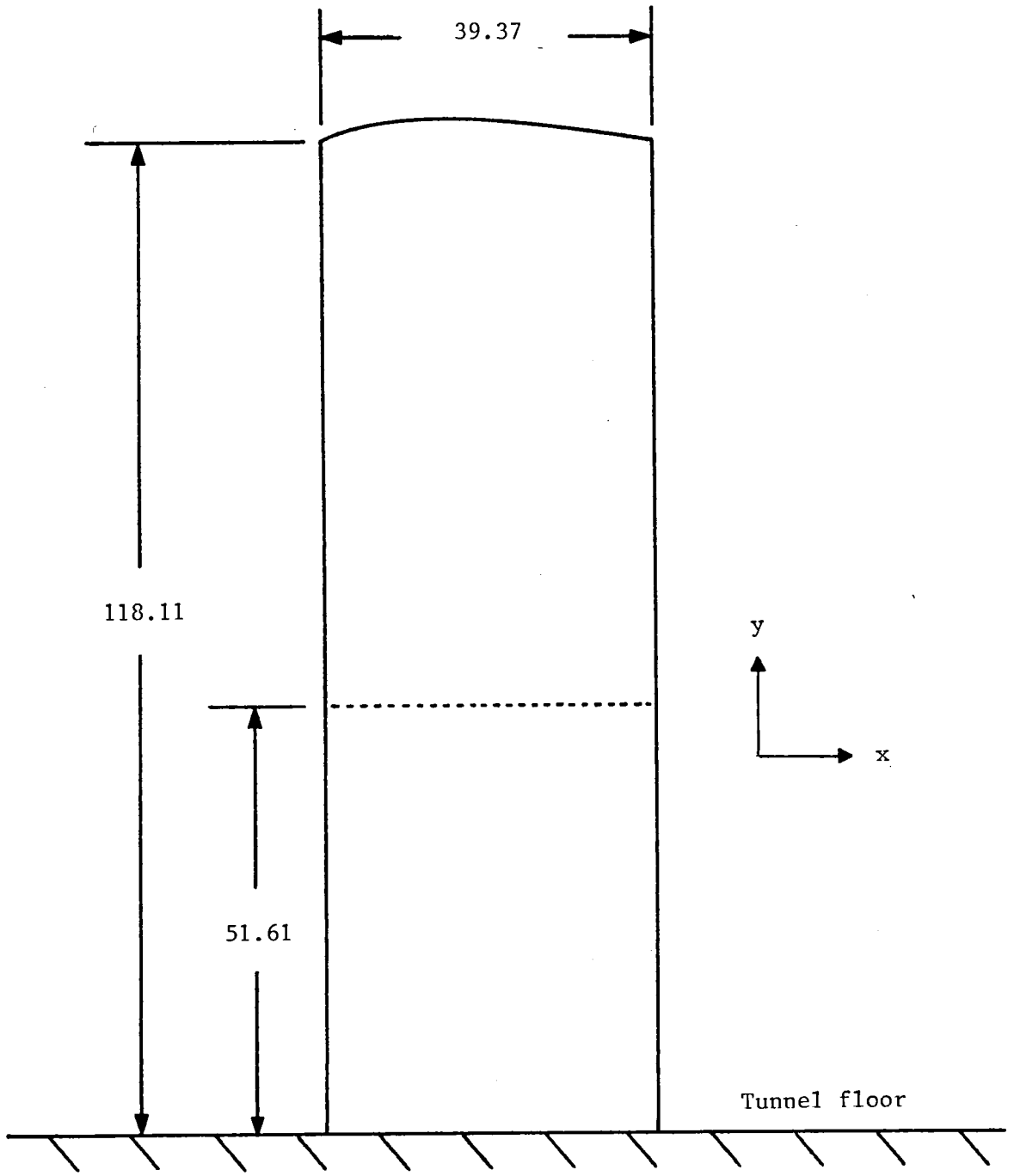


Figure 1. Sketch of model planform. Dimensions are in inches.

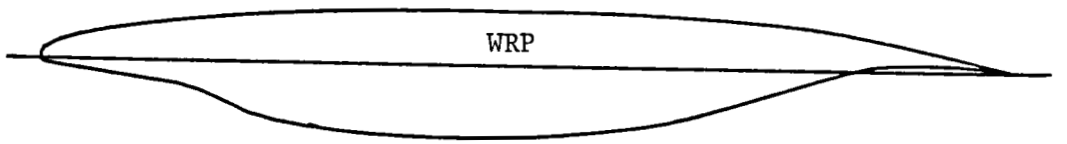


(a) Cruise configuration.

(b) Trailing-edge flap configuration.

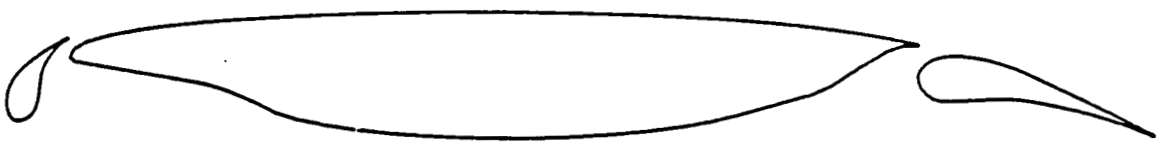

(c) 0.10$c$ leading-edge flap configuration.

(d) 0.12$c$ leading-edge flap configuration.

Figure 2. Section contours of wing configurations tested.


L-83-2625

(a) Photograph of cruise configuration.

Figure 3. Semispan wing model installed in the Langley 14- by 22-Foot Subsonic Tunnel.

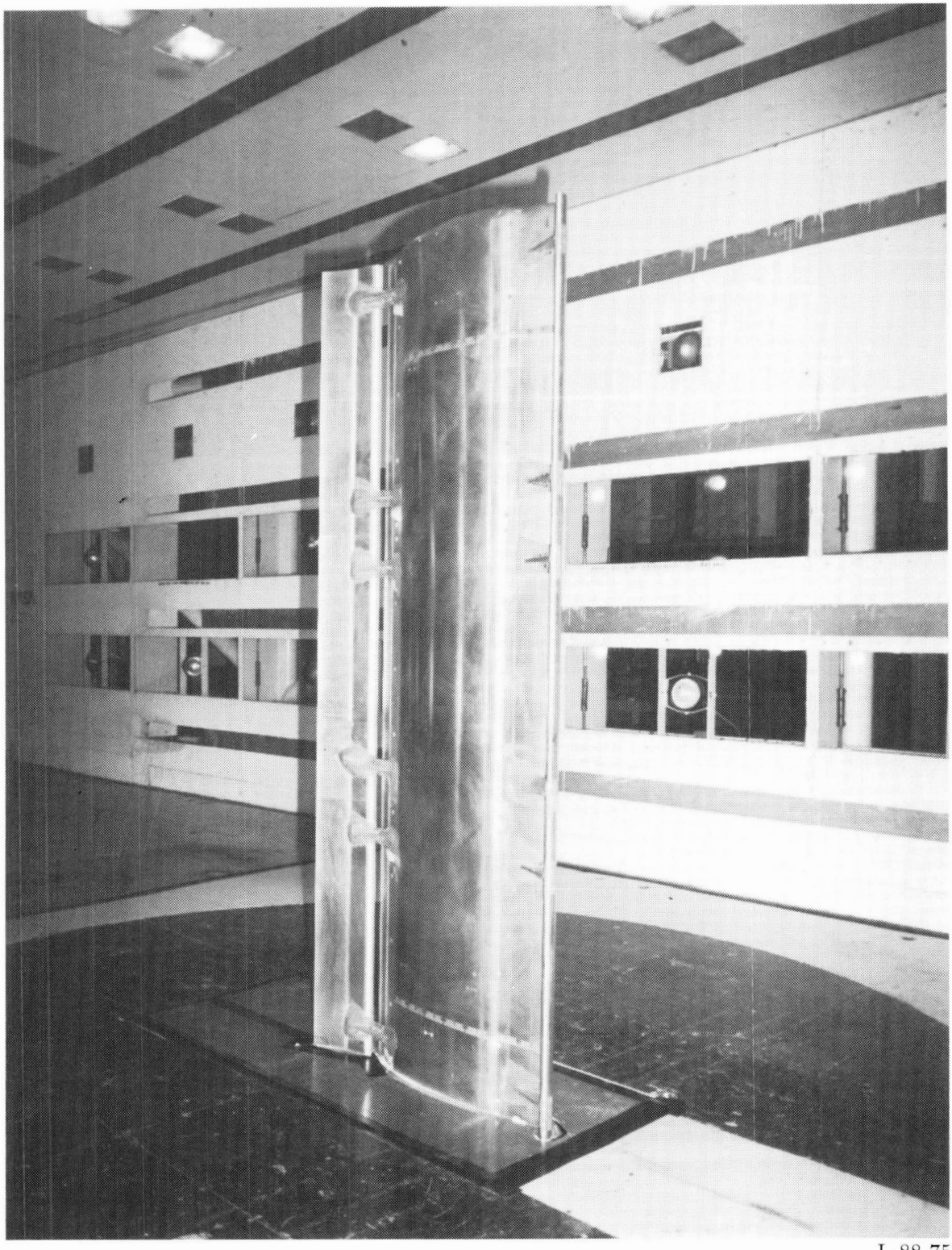

L-88-75

(b) Photograph of high-lift configuration.

Figure 3. Concluded.

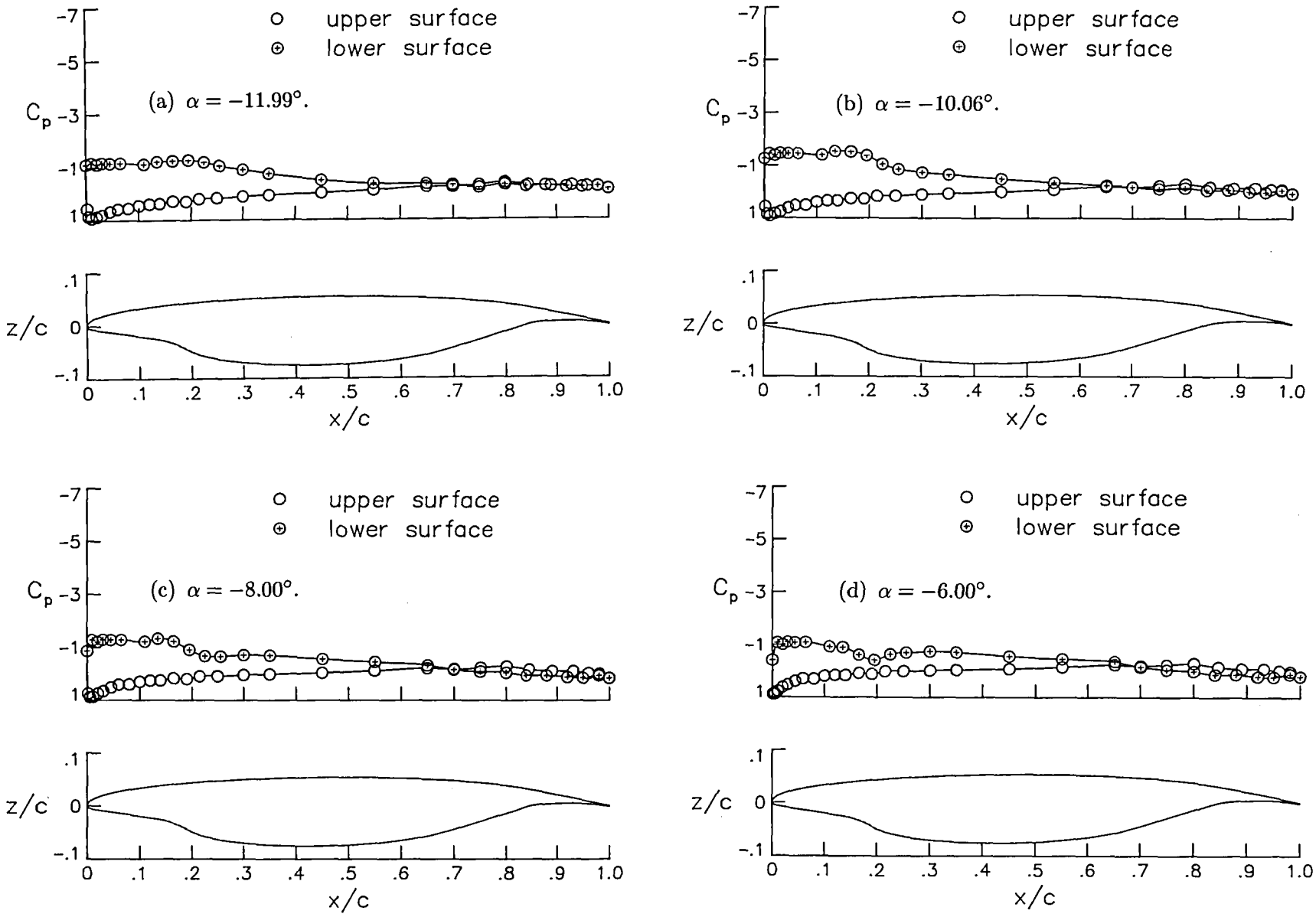


Figure 4. Pressure distribution data for cruise configuration with $q_\infty = 30$ psf. This figure is same as figure 9 in part 2.

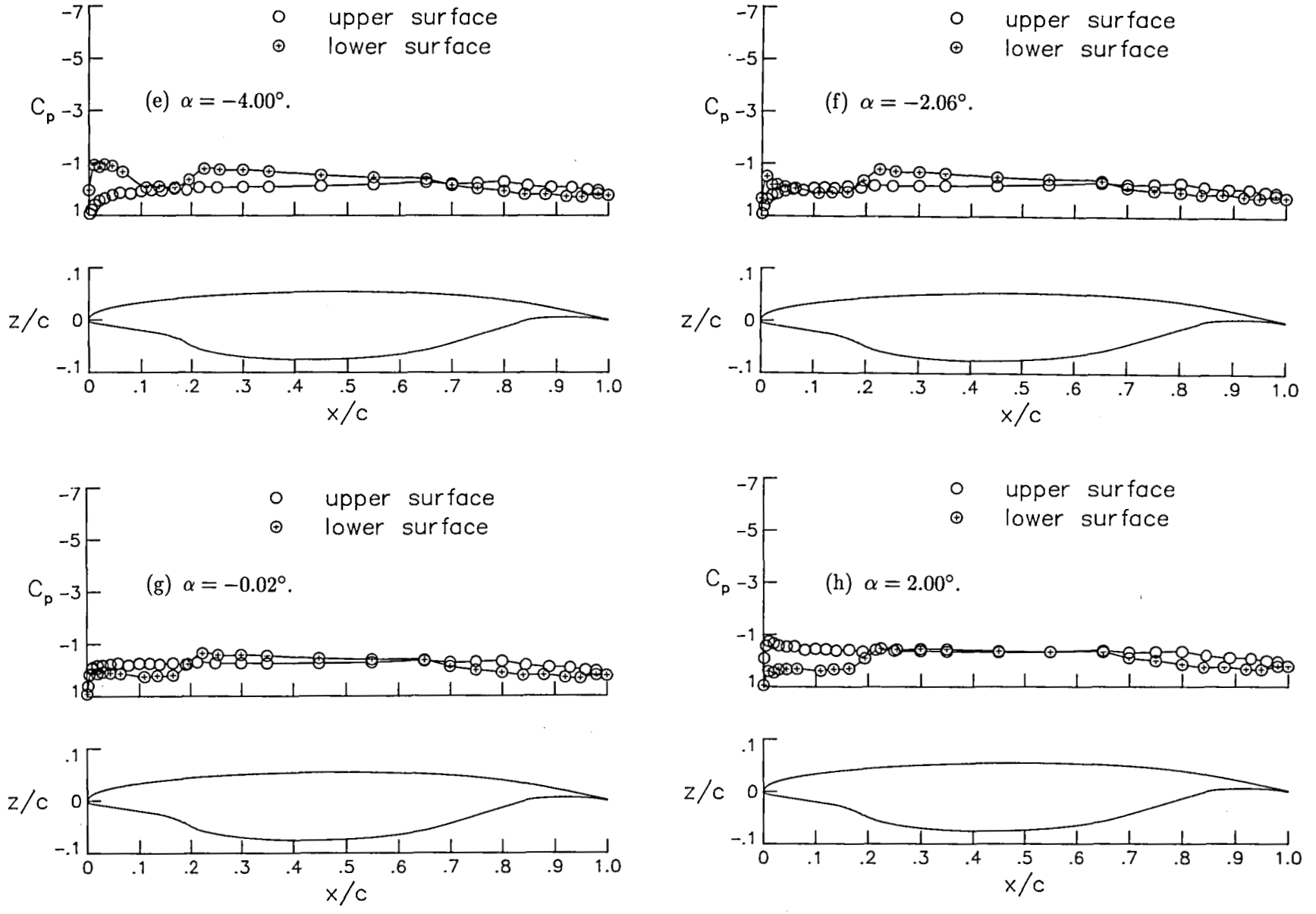


Figure 4. Continued.

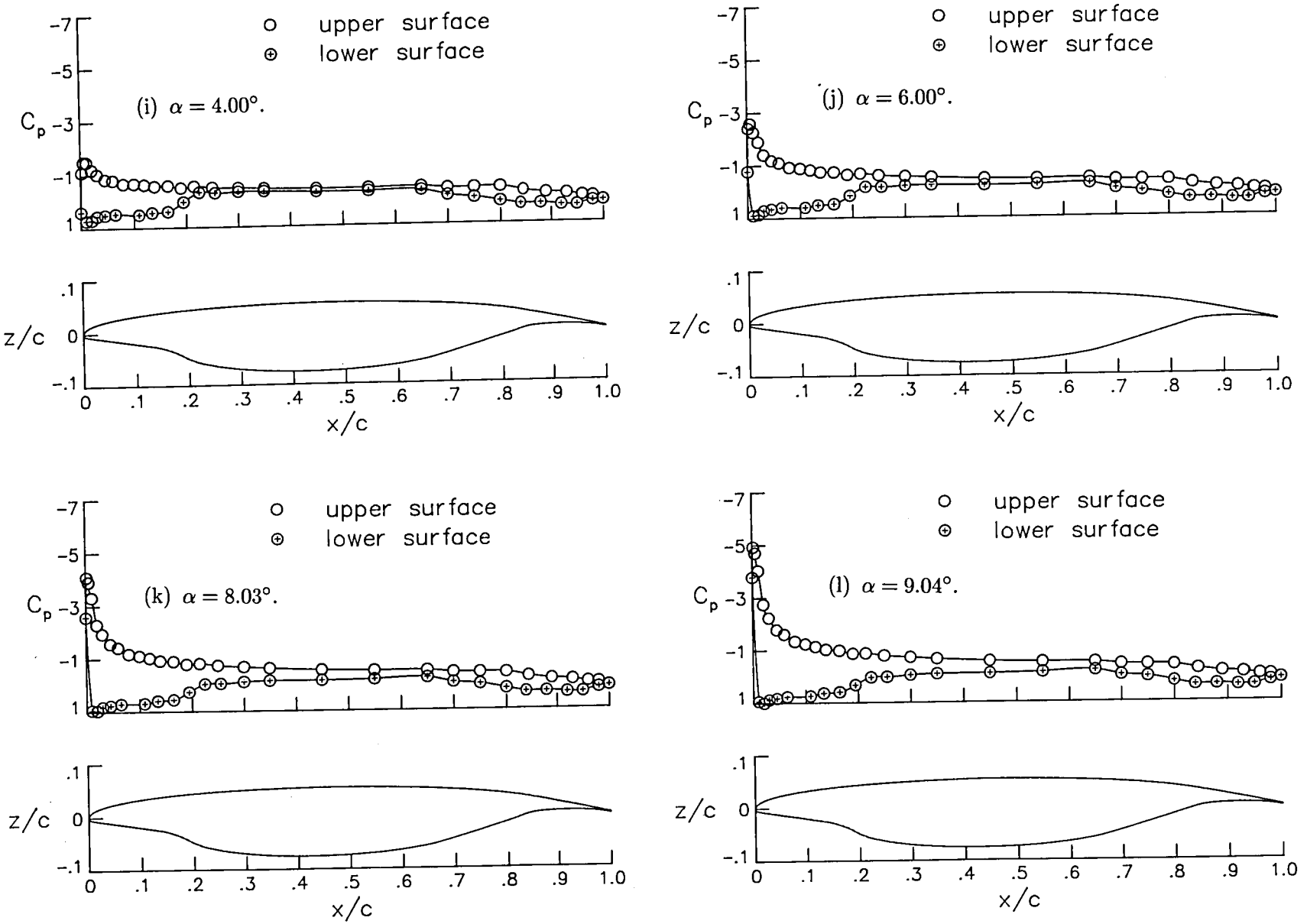


Figure 4. Concluded.

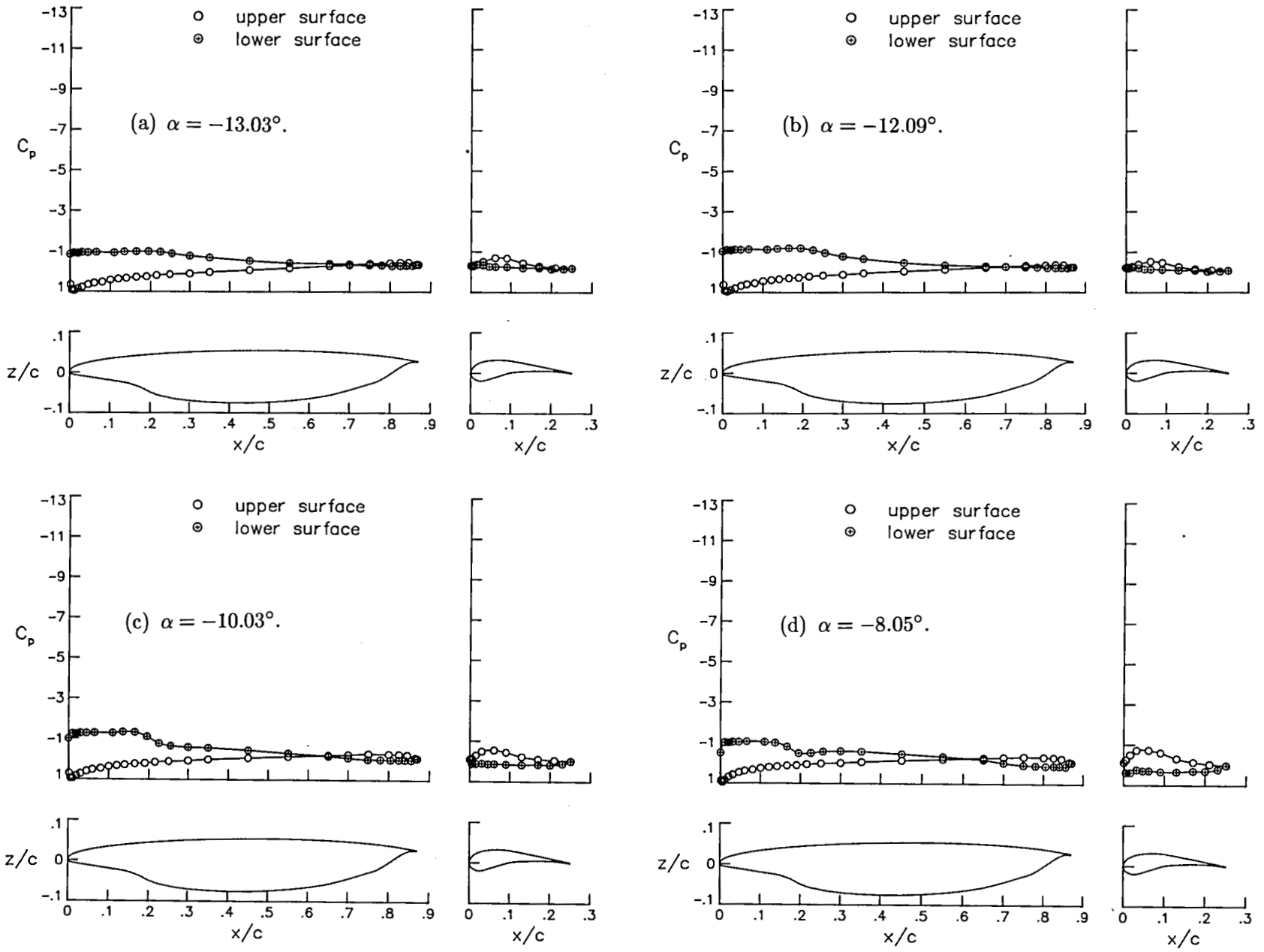


Figure 5. Pressure distribution data for trailing-edge flap configuration with $\delta_{TE} = 15°$ and $q_\infty = 30$ psf. This figure is same as figure 11 in part 2.

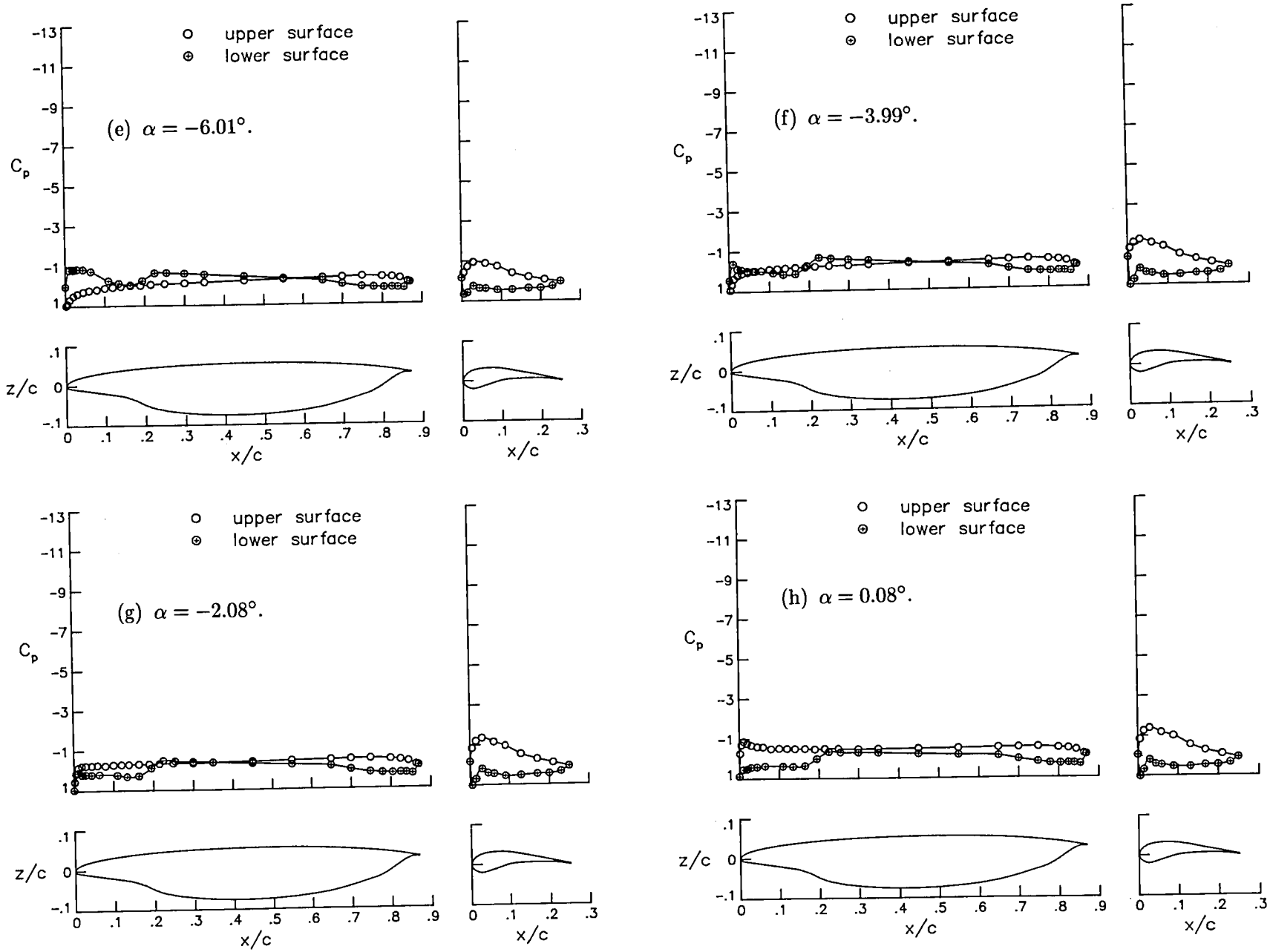


Figure 5. Continued.

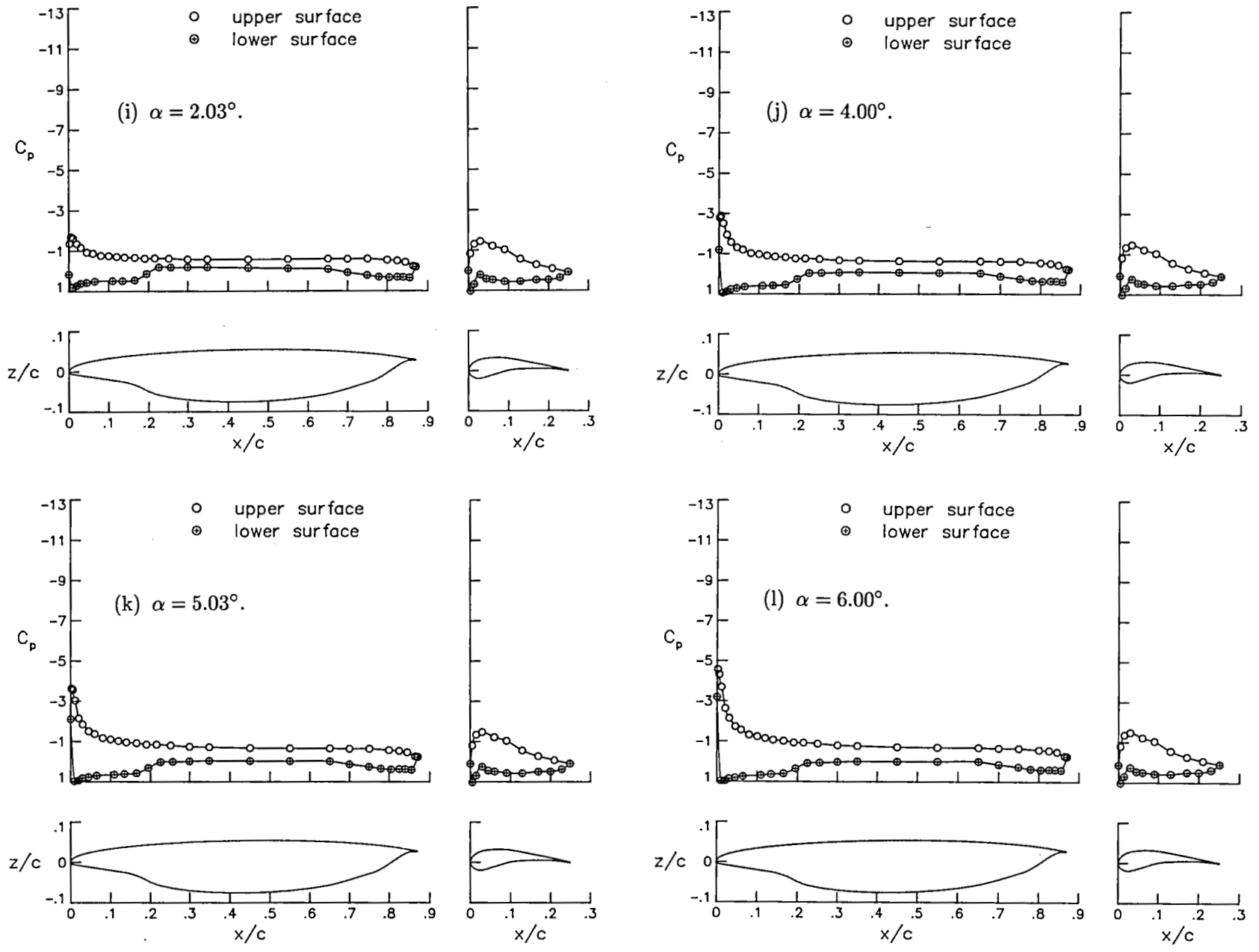


Figure 5. Continued.

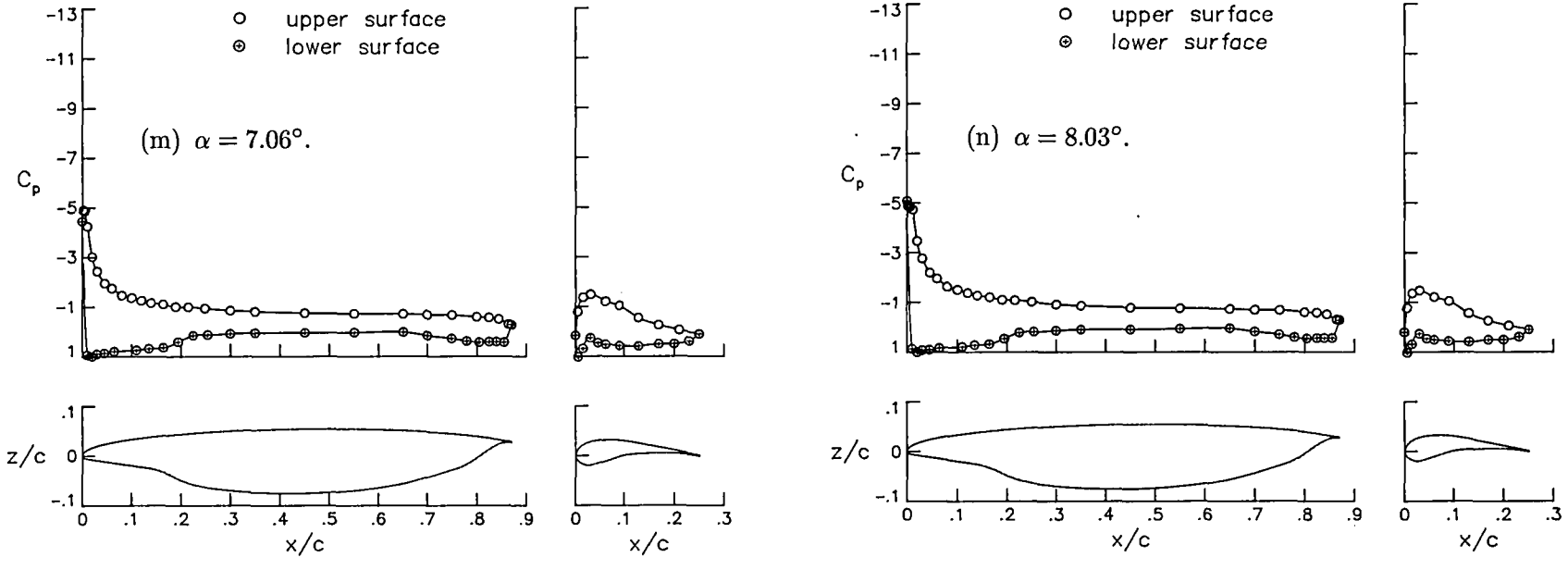


Figure 5. Concluded.

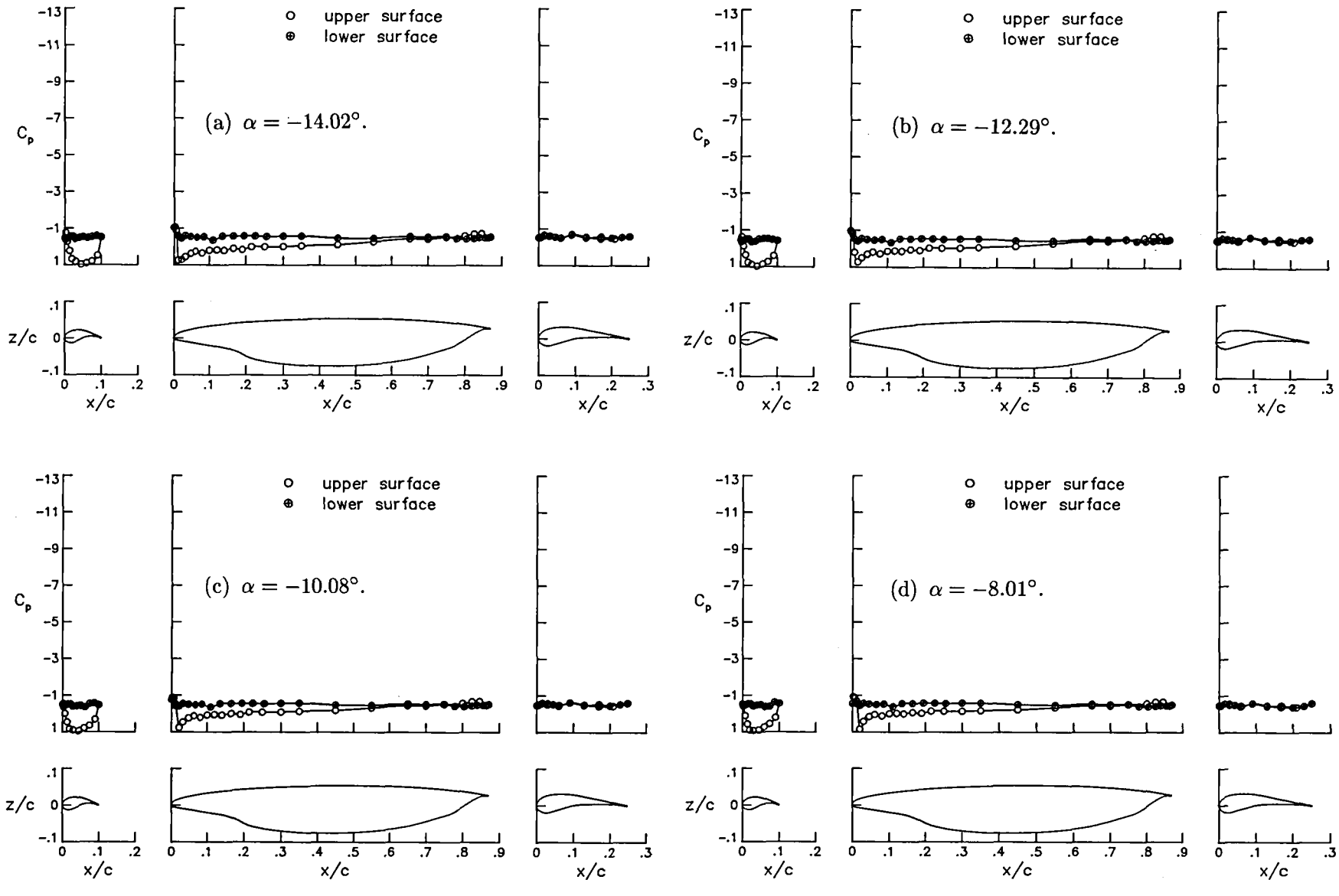


Figure 6. Pressure distribution data for trailing-edge flap with 0.10$c$ leading-edge flap configuration with $\delta_{LE} = -55°$, $\delta_{TE} = 30°$, and $q_\infty = 30$ psf. This figure is same as figure 19 in part 2.

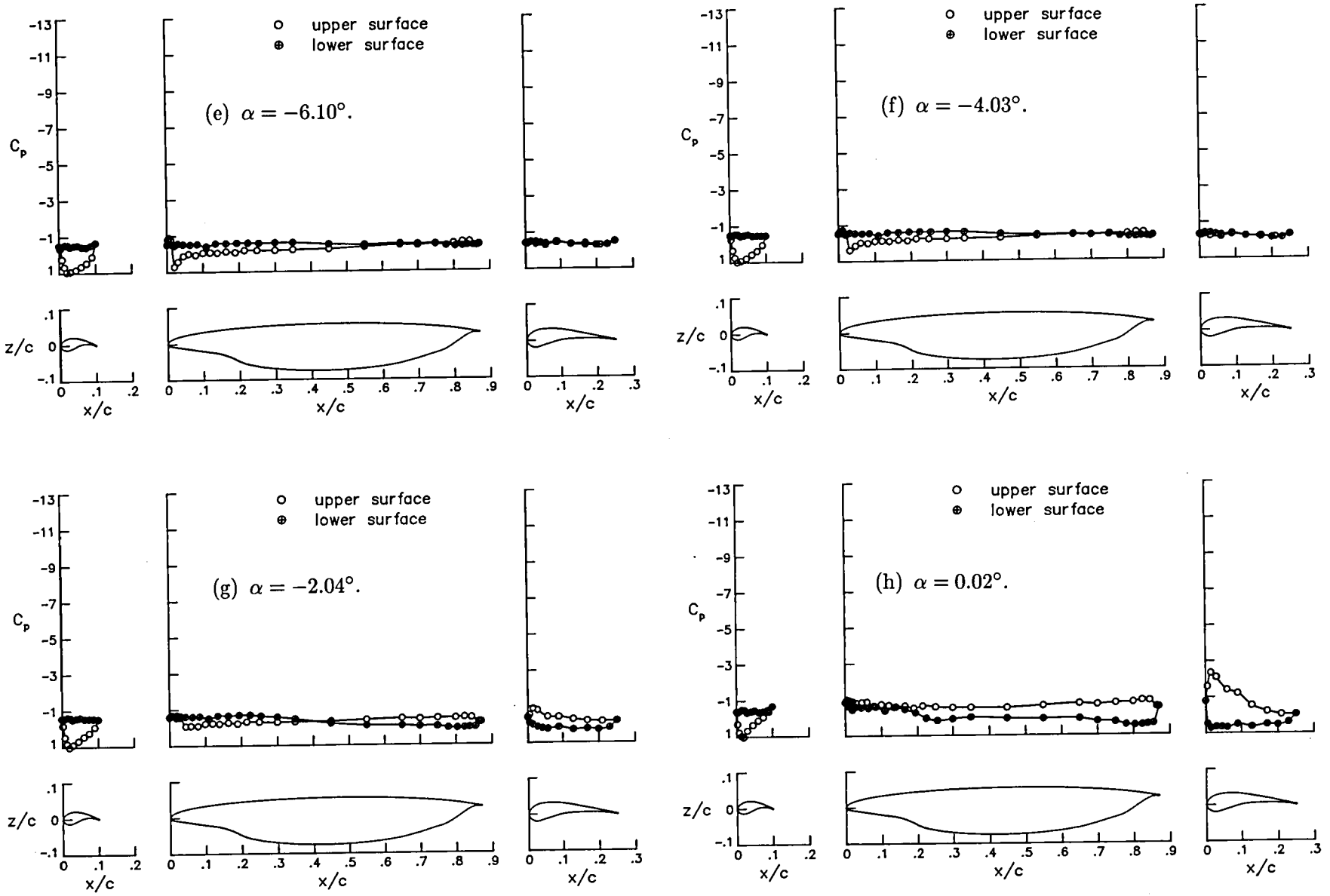


Figure 6. Continued.

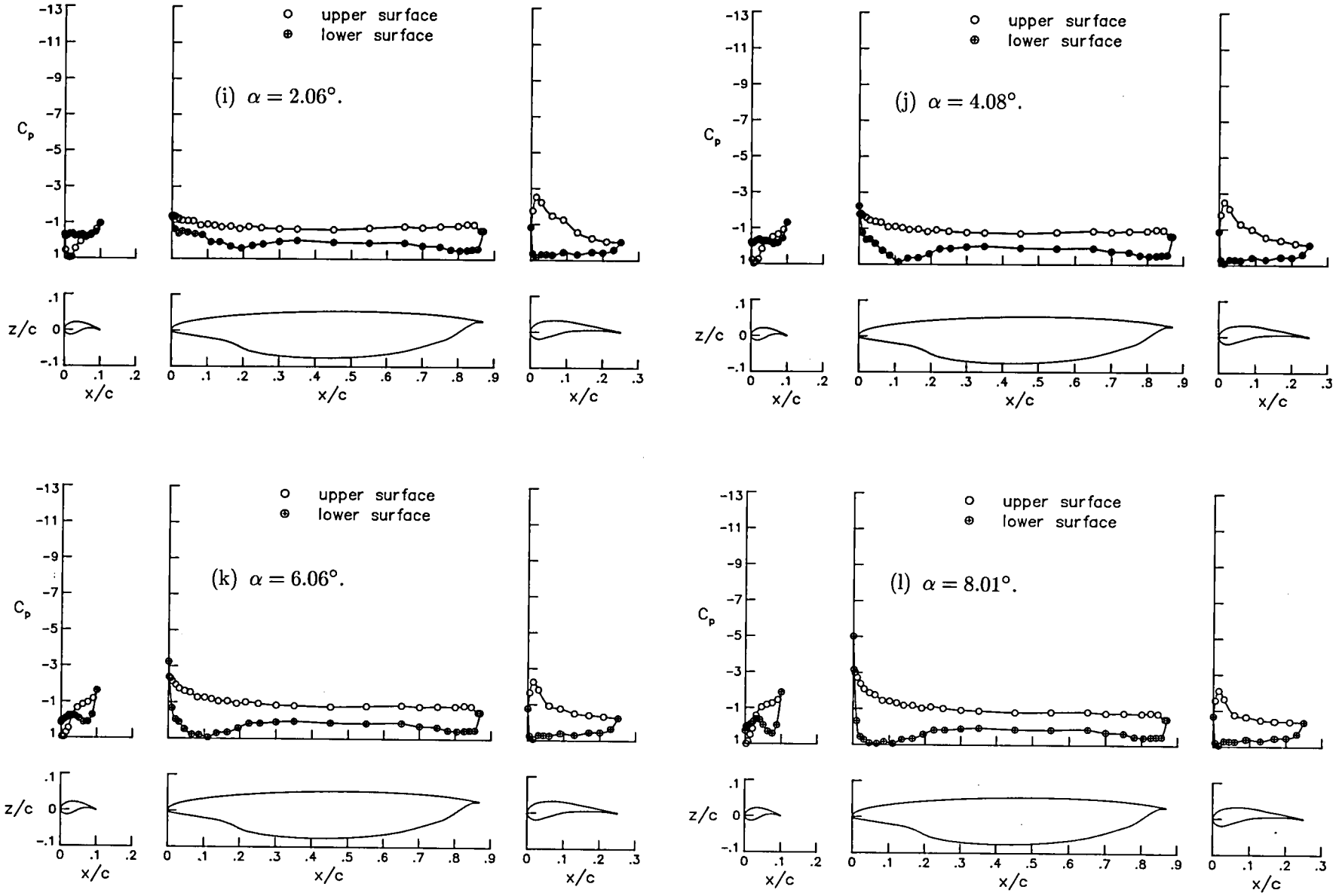


Figure 6. Continued.

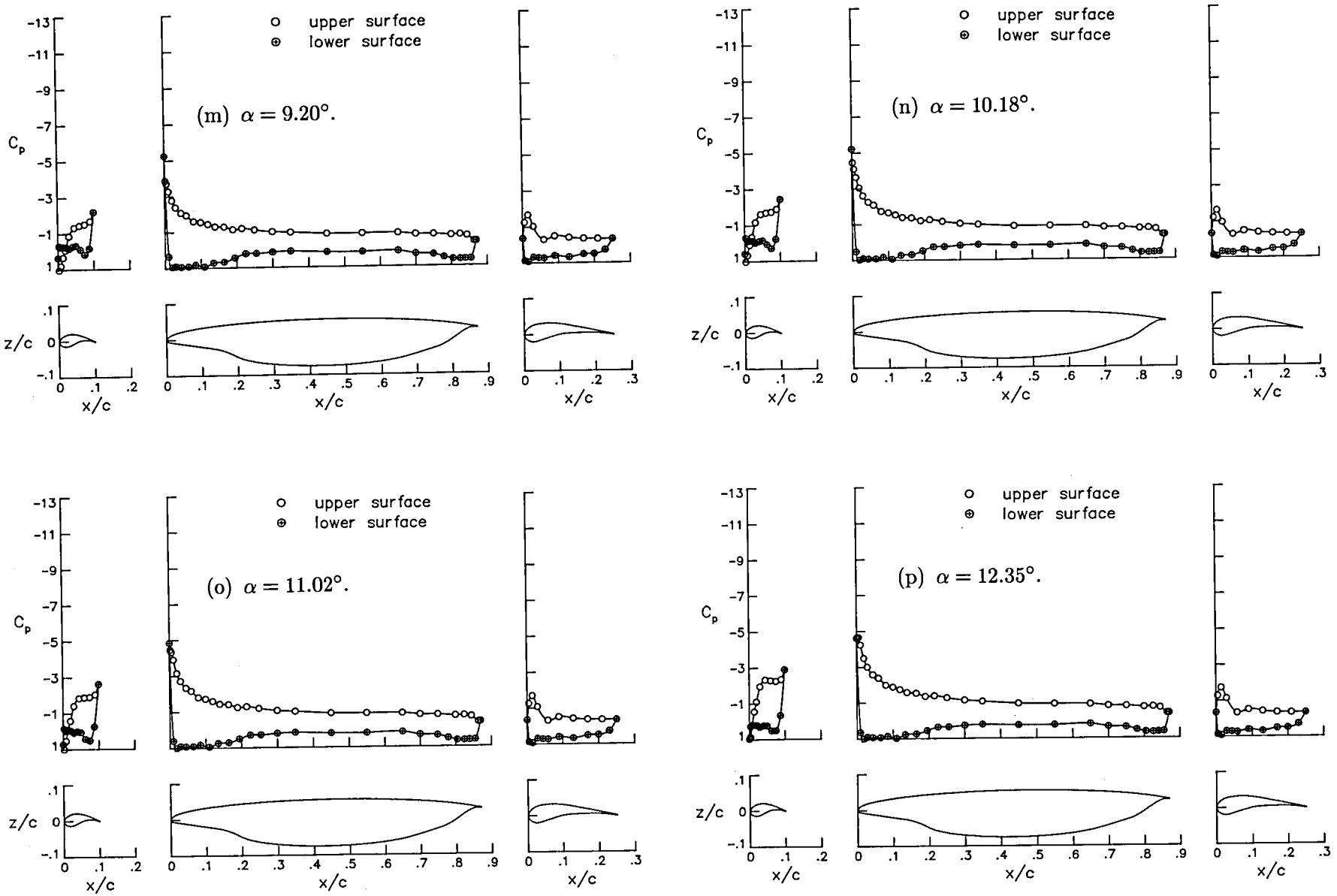


Figure 6. Continued.

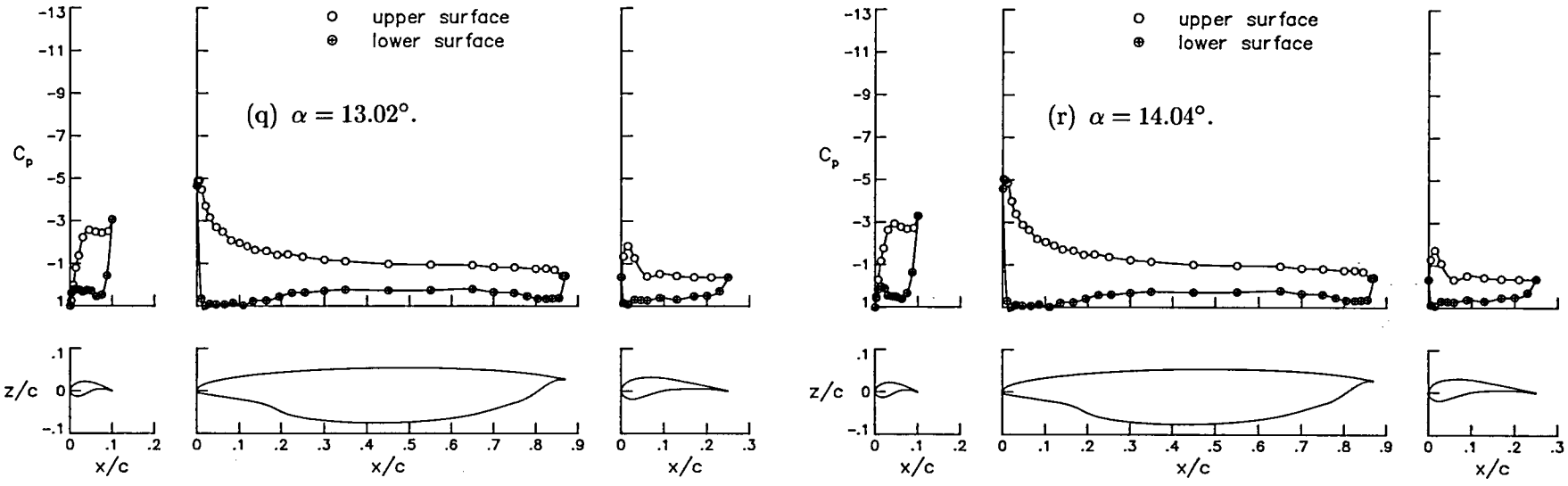


Figure 6. Concluded.

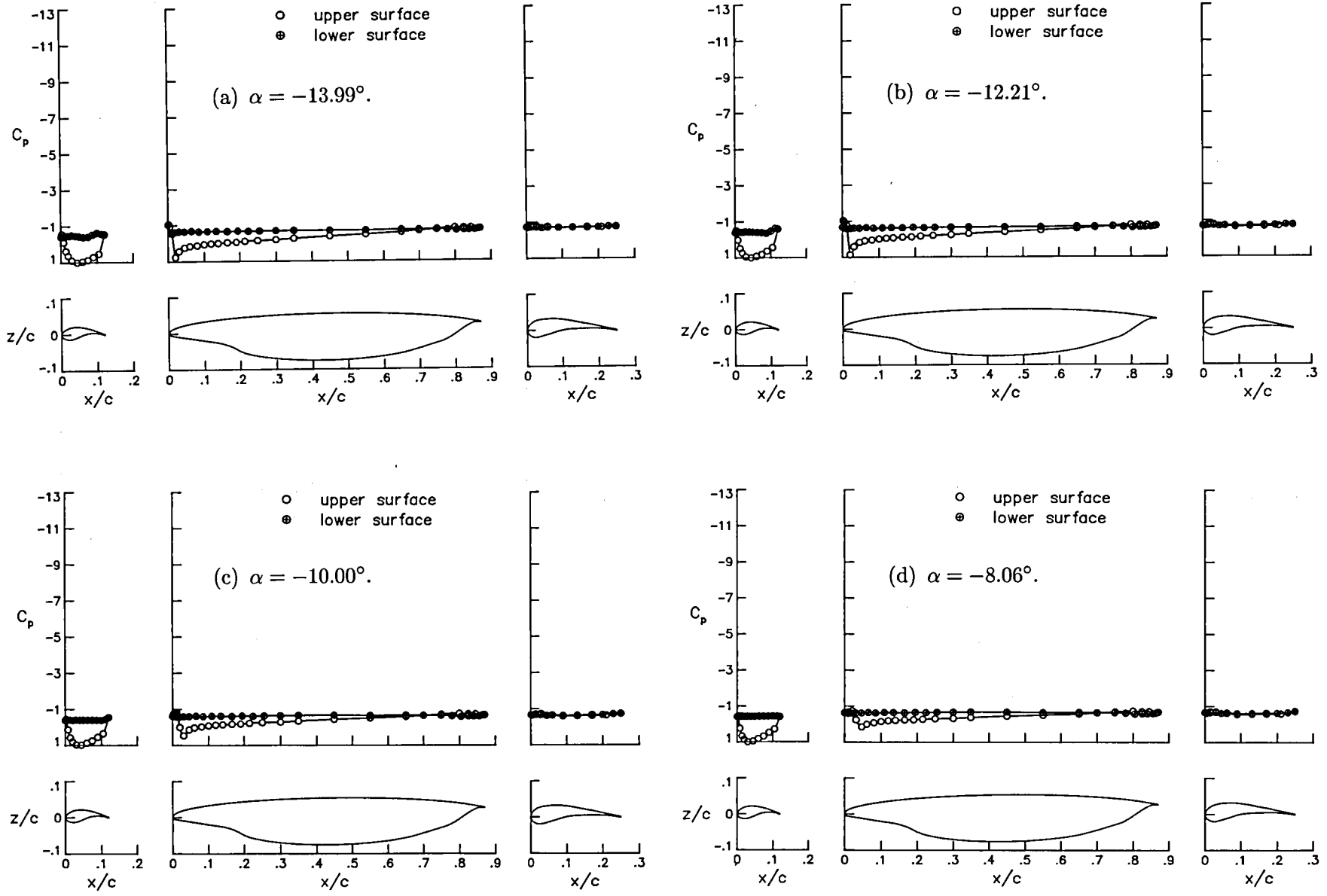


Figure 7. Pressure distribution data for trailing-edge flap with $0.12c$ leading-edge flap configuration with $\delta_{LE} = -55°$, $\delta_{TE} = 30°$, and $q_\infty = 30$ psf. This figure is same as figure 31 in part 2.

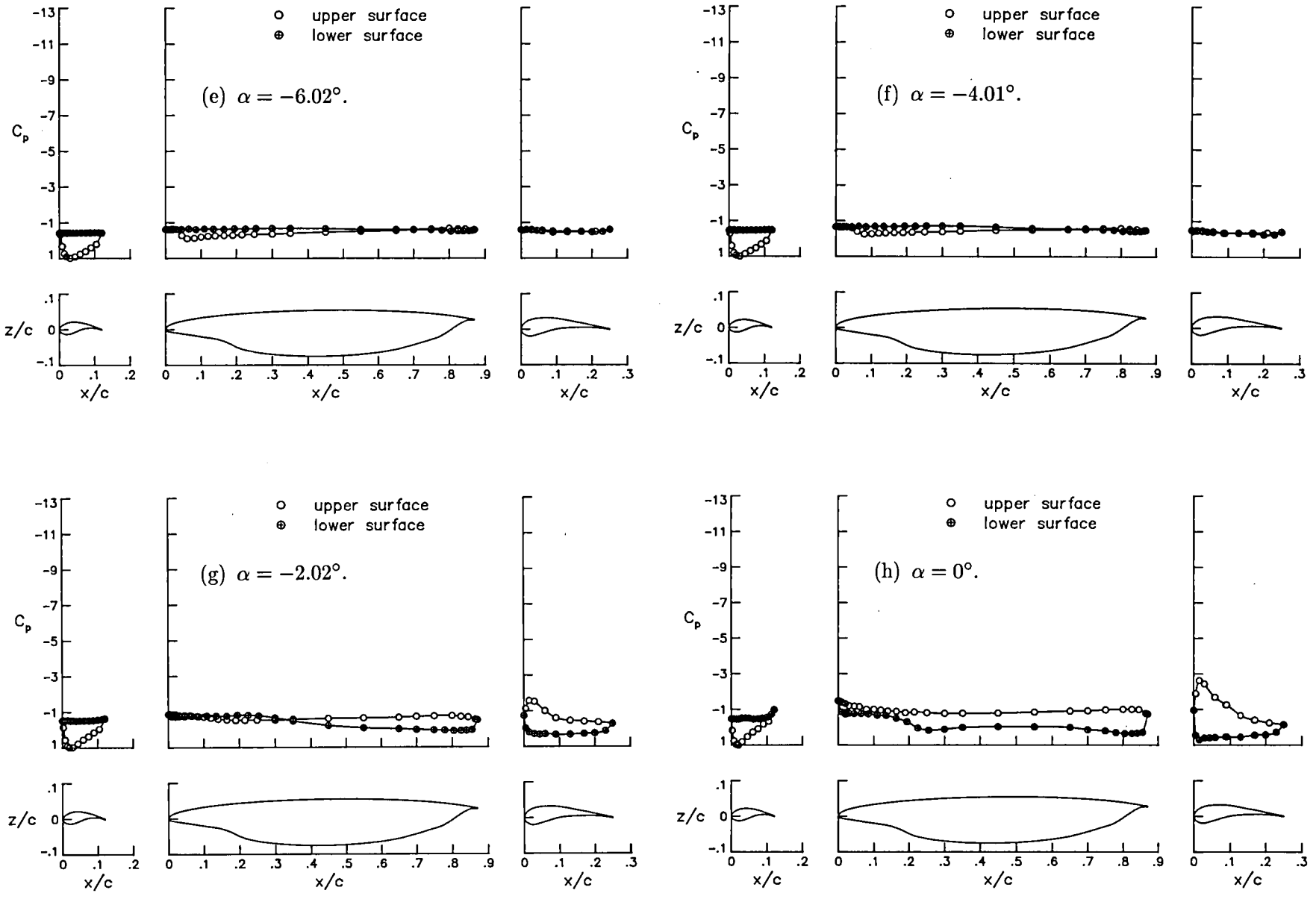


Figure 7. Continued.

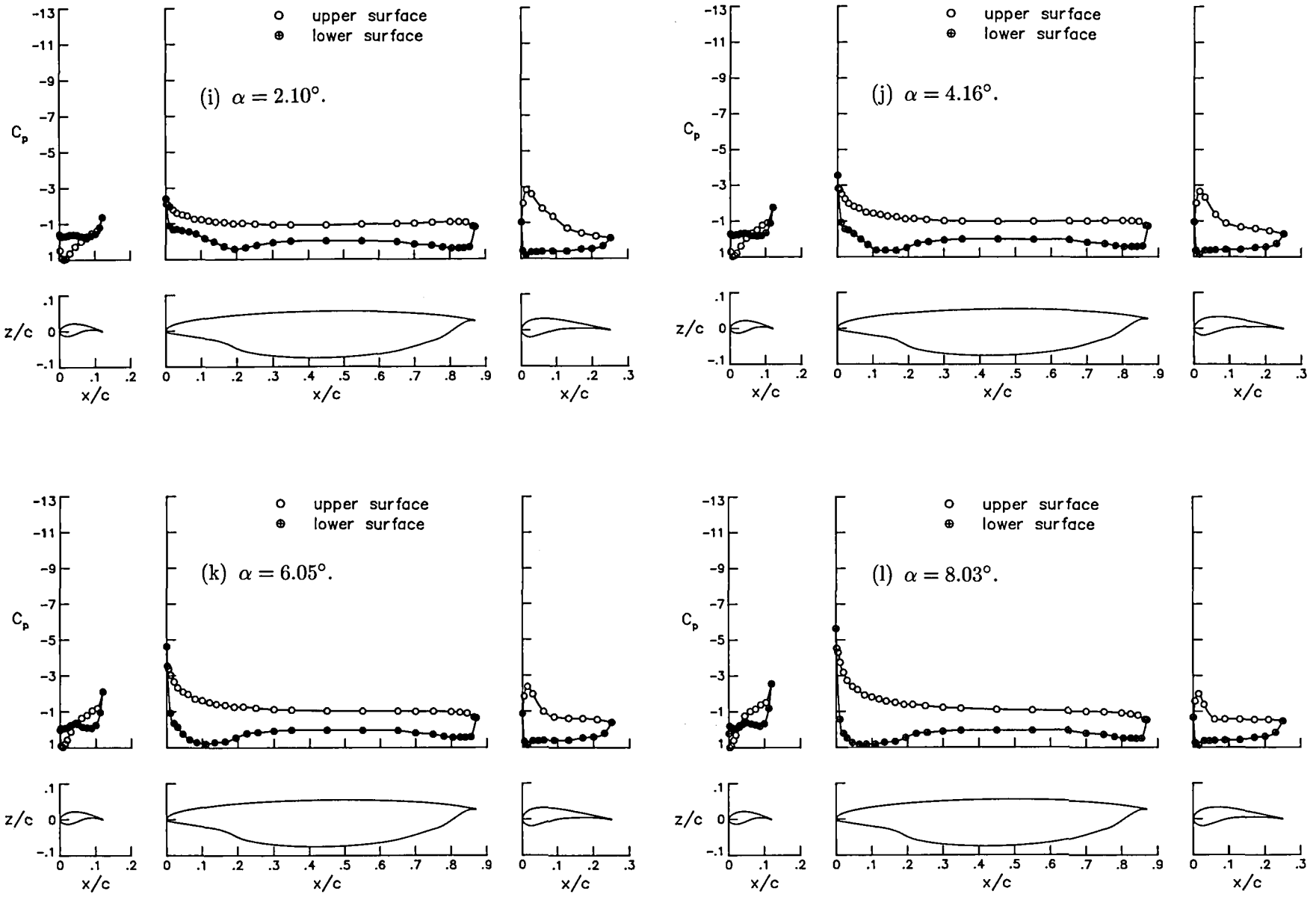


Figure 7. Continued.

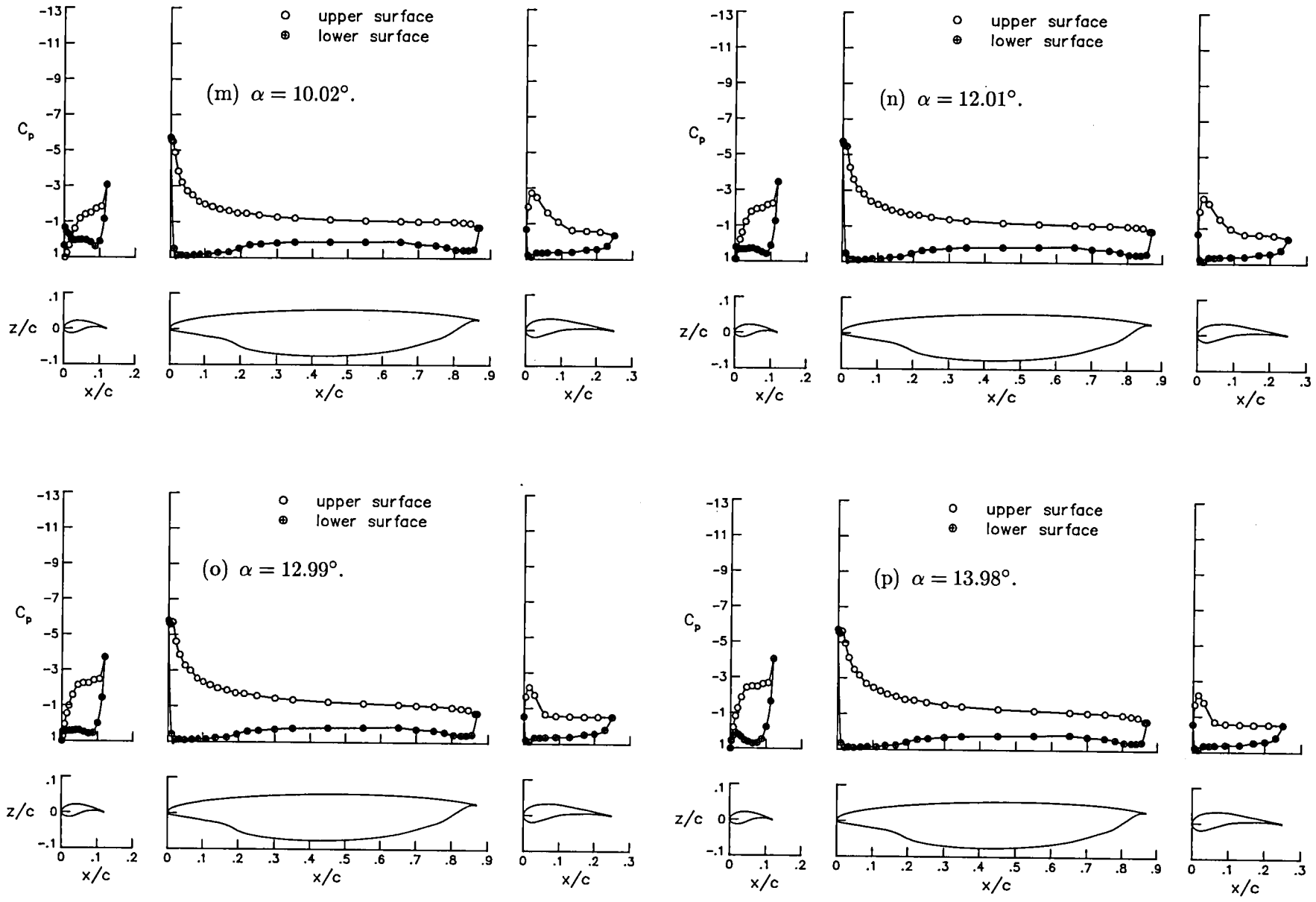


Figure 7. Continued.

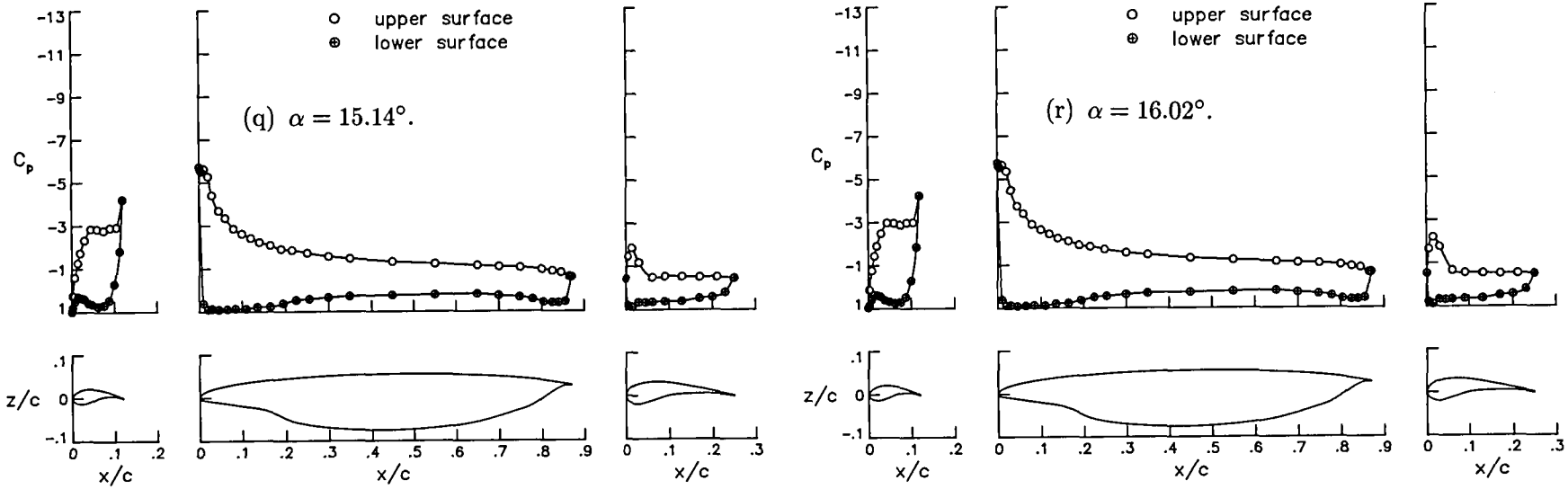


Figure 7. Concluded.

NASA
National Aeronautics and Space Administration

# Report Documentation Page

| 1. Report No. | 2. Government Accession No. | 3. Recipient's Catalog No. |
|---|---|---|
| NASA TM-4040, Part 1 | | |

| 4. Title and Subtitle | 5. Report Date |
|---|---|
| Pressure Distributions From Subsonic Tests of an Advanced Laminar-Flow-Control Wing With Leading- and Trailing-Edge Flaps | July 1988 |
| | 6. Performing Organization Code |
| 7. Author(s) | 8. Performing Organization Report No. |
| Zachary T. Applin and Garl L. Gentry, Jr. | L-16405 |
| 9. Performing Organization Name and Address | 10. Work Unit No. |
| NASA Langley Research Center<br>Hampton, VA 23665-5225 | 307-50-06-03 |
| | 11. Contract or Grant No. |
| 12. Sponsoring Agency Name and Address | 13. Type of Report and Period Covered |
| National Aeronautics and Space Administration<br>Washington, DC 20546-0001 | Technical Memorandum |
| | 14. Sponsoring Agency Code |

15. Supplementary Notes

16. Abstract

An unswept, semispan wing model equipped with full-span leading- and trailing-edge flaps was tested in the Langley 14- by 22-Foot Subsonic Tunnel to determine the effect of high-lift components on the aerodynamics of an advanced laminar-flow-control (LFC) airfoil section. Chordwise pressure distributions near the midsemispan were measured for four configurations: cruise, trailing-edge flap only, and trailing-edge flap with a leading-edge Krueger flap of either 0.10 or 0.12 chord. Part 1 of this report presents a representative sample of the plotted pressure distribution data for each configuration tested. Part 2 (under separate cover) presents the entire set of plotted and tabulated pressure distribution data. The data are presented without analysis.

| 17. Key Words (Suggested by Authors(s)) | 18. Distribution Statement |
|---|---|
| High-lift systems<br>Pressure distributions<br>Laminar-flow control | Unclassified—Unlimited<br><br>Subject Category 02 |

| 19. Security Classif.(of this report) | 20. Security Classif.(of this page) | 21. No. of Pages | 22. Price |
|---|---|---|---|
| Unclassified | Unclassified | 31 | A03 |

NASA FORM 1626 OCT 86

NASA-Langley, 1988

For sale by the National Technical Information Service, Springfield, Virginia 22161-2171